BMC Ecology and Evolution

RESEARCH

Open Access

Multi-modal locomotor costs favor smaller males in a sexually dimorphic leaf-mimicking insect

Romain P. Boisseau[1*], Thies H. Büscher[2], Lexi J. Klawitter[1], Stanislav N. Gorb[2], Douglas J. Emlen[1] and Bret W. Tobalske[1]

Abstract

Background: In most arthropods, adult females are larger than males, and male competition is a race to quickly locate and mate with scattered females (scramble competition polygyny). Variation in body size among males may confer advantages that depend on context. Smaller males may be favored due to more efficient locomotion leading to higher mobility during mate searching. Alternatively, larger males may benefit from increased speed and higher survivorship. While the relationship between male body size and mobility has been investigated in several systems, how different aspects of male body morphology specifically affect their locomotor performance in different contexts is often unclear.

Results: Using a combination of empirical measures of flight performance and modelling of body aerodynamics, we show that large body size impairs flight performance in male leaf insects (*Phyllium philippinicum*), a species where relatively small and skinny males fly through the canopy in search of large sedentary females. Smaller males were more agile in the air and ascended more rapidly during flight. Our models further predicted that variation in body shape would affect body lift and drag but suggested that flight costs may not explain the evolution of strong sexual dimorphism in body shape in this species. Finally, empirical measurements of substrate adhesion and subsequent modelling of landing impact forces suggested that smaller males had a lower risk of detaching from the substrates on which they walk and land.

Conclusions: By showing that male body size impairs their flight and substrate adhesion performance, we provide support to the hypothesis that smaller scrambling males benefit from an increased locomotor performance and shed light on the evolution of sexual dimorphism in scramble competition mating systems.

Keywords: Phasmatodea, Scramble competition, Flight, Adhesion, Computational fluid dynamics

Background

Sexual dimorphism is the ultimate result of sex-dependent selection leading traits toward different optima in each sex [1–3]. Many key hypotheses for the ultimate drivers of sexual dimorphism, and specifically sexual size dimorphism (SSD), remain controversial or relatively poorly supported [2]. While factors favoring larger bodies are widely recognized—i.e., fecundity selection in females [4, 5] and sexual selection in males [6]—the selective pressures favoring smaller sizes have received less attention [2, 3, 7–9]. In resource or female defense mating systems, the largest, most armored males are often favored against rivals over access to mating [6, 10–13]. However, when females are sedentary and dispersed throughout the landscape and do not rely on an easily defensible

*Correspondence: romain.boisseau@umontana.edu
[1] Division of Biological Sciences, University of Montana, 32 Campus Dr, Missoula, MT 59812, USA
Full list of author information is available at the end of the article

resource, male competition unfolds instead as a race to locate females (i.e., scramble competition polygyny) [14]. In this context, selection is predicted to favor male traits that increase the distance travelled during mate searching (i.e., mobility) [14].

Small and slender bodies are often assumed to be beneficial for the searching performance and mating success of scrambling males, as studies have shown in several systems [8, 9, 15–18]—e.g., by increasing endurance and enabling longer searching times, eventually leading to higher encounter rates with females [19]. For instance, in aerial species, wider and heavier bodies, which produce more aerodynamic drag and have a higher wing loading (i.e., $\frac{body\ weight}{wing\ area}$), are usually thought to reduce flight performance as they require relatively more power to be maintained in the air, particularly during hovering or slow forward flight [20]. The "Ghiselin–Reiss small-male hypothesis" specifically suggests that males are usually smaller than females in scrambling systems because of the time allocation trade-off between foraging versus mate searching [9, 21]. Because small males require less energy to fuel their activities, they can spend relatively more time searching for mates and less time feeding. Such a trade-off has been shown empirically in water striders where smaller males have a greater mating success when food is limited [17]. However, directional selection for smaller sizes does not appear universal among scrambling systems [14]. In some species, it is the larger males that are more mobile and more successful than smaller counterparts, possibly owing to higher survivorship during mate searching, higher movement speeds or larger, more effective sensory structures [22, 23]. Identifying how different aspects of locomotion are affected by body morphology is therefore critical to understand the variation of the effect of body size and shape on mobility. In the present study, we tested the hypothesis that smaller flying males have multiple locomotor advantages during mate searching in a scramble-competition insect species with pronounced sexual dimorphism. We also investigated the role of body shape per se in male flight performance to test the related hypothesis that males benefit from being slenderer in addition to being smaller.

We quantified the effects of variation in morphology (body size and shape) on flight and substrate attachment performance in male leaf insects (*Phyllium philippinicum*, Hennemann, Conle, Gottardo & Bresseel, 2009, Phylliidae, Phasmatodea). In this solitary canopy-dwelling species, large, sedentary adult females are outstanding leaf-mimics due to lateral 'leaf-like' expansions of the abdominal segments and legs [24–26]. Adult males are nine times lighter and almost two times slenderer than females, and have relatively longer antennae (i.e., strong size [SSD] and shape dimorphism; Fig. 1). Adult females lack hindwings but have extended forewings that lie flat on their dorsum, aiding in camouflage [24]. These wings cannot flap but can contribute to parachuting if falling. In contrast, adult males have rudimentary forewings and long, fully-developed transparent hindwings allowing flapping flight. Males use their long antennae to detect pheromones and actively search for sedentary females widely scattered in the canopy [27]. Although the natural history of these nocturnal insects is largely unknown in the field, phylliid males are often observed flying to light traps [28] and are very active at night in captivity—i.e., climbing on branches and readily taking off when reaching the top of a stem [29–32]. In our lab cultures, *P. philippinicum* males quickly initiate copulation after finding a female, which typically lasts for more than 3 h, and then stay on the back of the female for the following day before resuming a period of high nocturnal activity. In contrast, females are sedentary, moving only to adjacent leaves to feed. These observations are consistent with a male-searching scramble competition mating system, and clearly suggest that mobility and specifically flight and substrate attachment performance (when walking and/or landing) may be critical for male fitness [14]. The complex 3D structure of the high canopy environment made of foliage, branches and substantial gaps [33, 34] and its aerodynamic characteristics—e.g., wind gusts [35]—likely select for greater agility and ascending performance in the air as well as a strong tarsal attachment performance to safely hold on to a wide variety of substrates when walking or landing.

We predicted that increases in body weight would impair flight performance (agility and ascending) [36, 37], and reduce the ability of these insects to hold on to branches or leaves when they walk or land, increasing the risk of crashing and falling from high perches. We also hypothesized that selection for efficient locomotion in males (higher lift:drag ratios, lower power requirements) in parallel with fecundity selection in females [5], could account for the extensive sexual dimorphism in body shape (the "skinniness" of males relative to females). As these insects fly at high body angles of attack, we predicted that wide 'leaf-like' body silhouettes would have proportionally greater drag and, hence, a lower lift to drag ratio, requiring relatively more mechanical work for flying and putting wider males at a locomotor disadvantage. We tested these predictions using an integrative approach combining scaling of gross morphology, micro-structure descriptions, empirical measures of flight and attachment, and modeling of flight costs and landing forces.

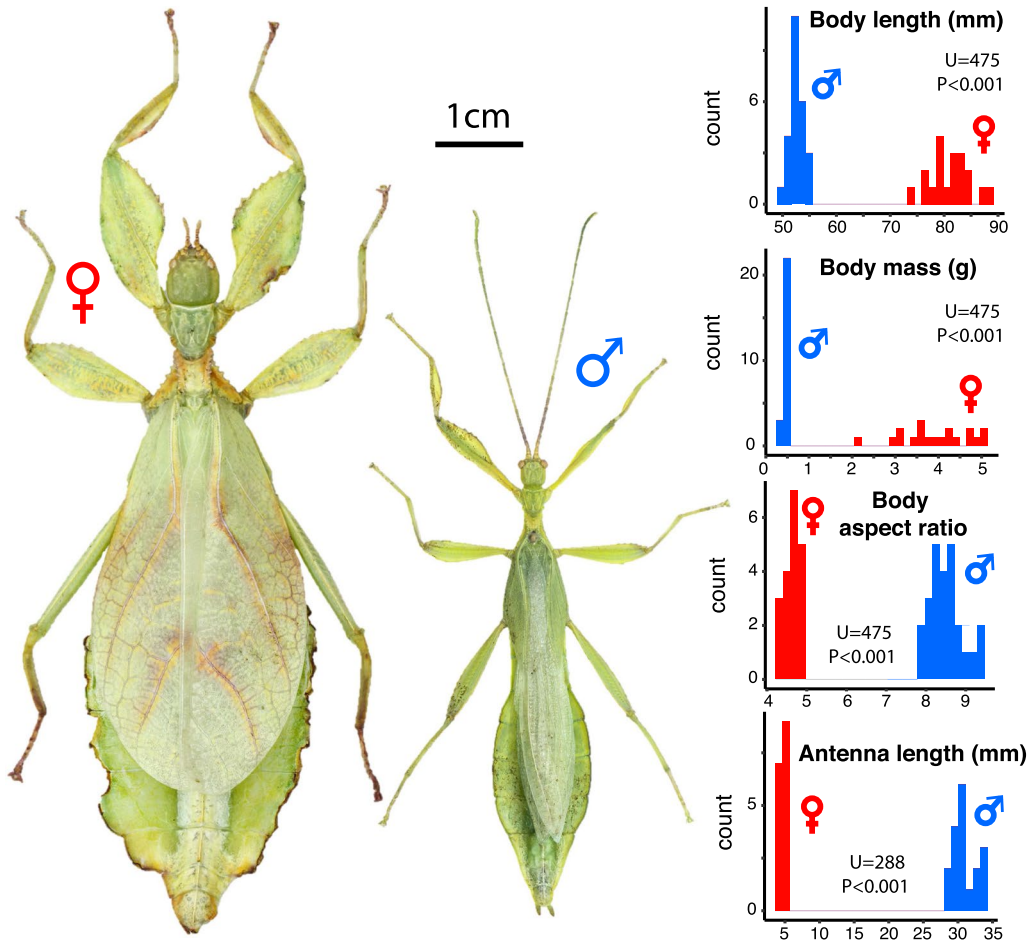

Fig. 1 Sexual dimorphism in *P. philippinicum*. Pictures display an adult female (left) and male (right) in dorsal view. Distributions of male (blue) and female (red) body length, mass, aspect ratio and antenna length are shown on the right. Wilcoxon–Mann–Whitney tests are presented to compare the two sexes

Results

Small males were more agile and climbed faster during flight than larger males

Compared to females, male *P. philippinicum* are shorter, lighter, skinnier and have much longer antennae (Fig. 1, Additional file 1: Figs. S1, S2). The large, leaf mimicking females are incapable of flight. For males, wing loading ($\frac{body\ weight}{wing\ area}$) increased significantly with body length (BL) (Additional file 1: Fig. S2H, Table S1) but relative flight muscle mass did not (Additional file 1: Fig. S2I, Table S1), indicating that large males were not compensating for their relatively heavier weight by building disproportionately large wings or flight muscles. This resulted in a substantial reduction in flight performance, which we empirically assessed using high-speed (500 fps) video recordings of flight trajectories (Additional file 1: Fig. S3, Additional file 2: Video S1, Additional file 3: Video S2 and Additional file 4: Video S3).

We first measured the rotational velocity of the insect long-axis body angle (i.e., pitch) when recovering from being dropped (see "Materials and methods", Additional file 1: Fig. S4B)[38]. The rotation occurred over multiple wingbeats (Additional file 2: Video S1, Additional file 3: Video S2), so we interpret it to represent torsional agility, an aspect of aerial maneuverability that reflects how fast the animal can correct its body pitch in the air from a free falling, head first, position to a stable body pitch [39, 40]. This is distinct from oscillation in body pitch within and among wingbeats which may reflect longitudinal instability and a lack of control [41]. We also measured mean horizontal and vertical velocity of the body center of mass to quantify the capacity of the individual to fly forward and ascend. Body mass

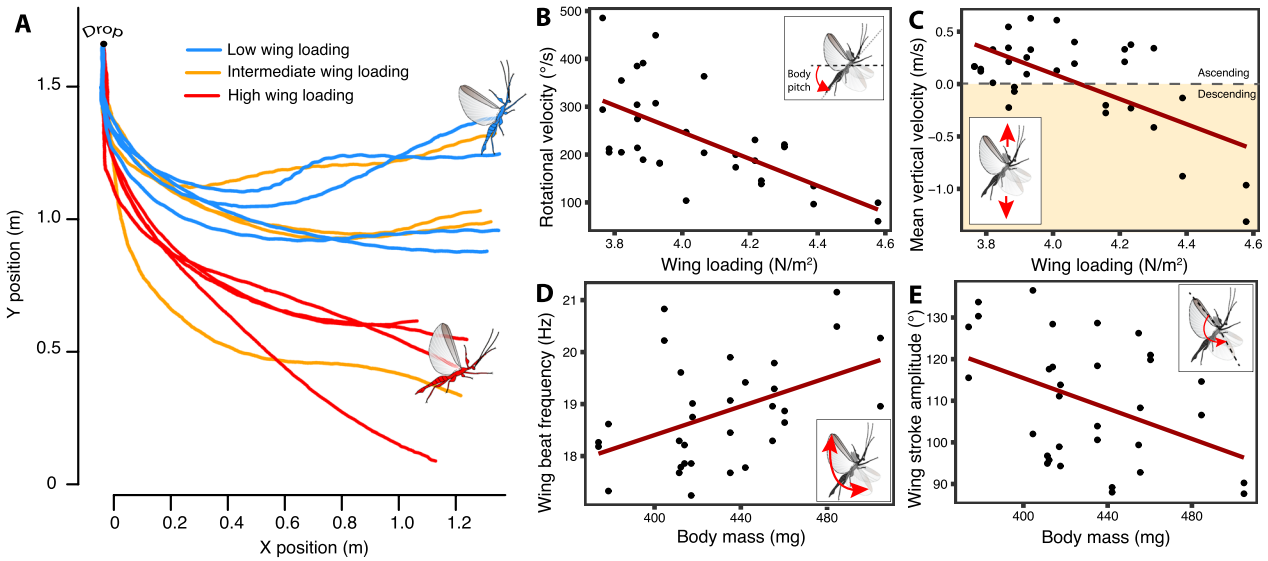

Fig. 2 Effect of body mass and wing loading on male *P. philippinicum* flight performance. **A** Flight trajectories of a subset of males with low (< 4 N m^{-2}), intermediate (4 < WL < 4.22 N m^{-2}) and high (> 4.22 N m^{-2}) wing loading. Rotational velocity (**B**) and mean vertical velocity (**C**) as a function of wing loading. Wingbeat frequency (**D**) and wing stroke amplitude (**E**) as a function of body mass. Mixed effect linear regressions including individual ID as a random factor are fitted in **B**–**E**. Each dot represent a flight trial (two per individual)

and wing area had significant opposing effects on rotational velocity and on mean vertical velocity (Table 1). Consistently, wing loading negatively affected rotational velocity ($\chi^2 = 13.0$, df = 1, p = 0.0003, Fig. 2B) and mean vertical velocity ($\chi^2 = 11.4$, df = 1, p = 0.0007, Fig. 2C). Thus, lighter males with relatively larger wings—i.e., with a lower wing loading—were both more adept at changing body pitch angle in the air and had a greater capacity for ascending flight than heavier males with relatively smaller wings (Fig. 2A). Despite flapping their wings at a higher frequency (Table 1, Fig. 2D), larger males also decreased stroke amplitude

Table 1 Analyses of the effects of body mass, wing area and body aspect ratio on various components of flight performance

Response variable	Fixed effects	β ± SE	Df	χ^2	p
Rotational velocity (° s^{-1})	**Body mass**	**−82.7 ± 25.2**	**1**	**7.04**	**0.008**
	Wing area	**53.6 ± 22.9**	**1**	**5.99**	**0.014**
	Body aspect ratio	13.4 ± 19.3	1	0.63	0.43
Mean vertical velocity (m s^{-1})	**Body mass**	**−0.37 ± 0.12**	**1**	**7.49**	**0.006**
	Wing area	**0.22 ± 0.10**	**1**	**4.99**	**0.025**
	Body aspect ratio	0.05 ± 0.09	1	0.40	0.53
Mean horizontal velocity (m s^{-1})	Body mass	0.23 ± 0.17	1	1.56	0.21
	Wing area	−0.10 ± 0.15	1	0.49	0.49
	Body aspect ratio	0.07 ± 0.13	1	0.44	0.51
Wing beat frequency (Hz)	**Body mass**	**0.51 ± 0.29**	**1**	**4.99**	**0.03**
	Wing area	0.26 ± 0.26	1	1.20	0.27
	Body aspect ratio	**0.43 ± 0.22**	**1**	**4.34**	**0.04**
Wing beat amplitude (°)	**Body mass**	**−2.59 ± 4.37**	**1**	**4.55**	**0.03**
	Wing area	−6.12 ± 3.97	1	2.93	0.09
	Body aspect ratio	−0.91 ± 3.36	1	0.10	0.75

The table shows a summary of linear mixed effect model outputs including individual ID as a random factor (N = 32 trials, 16 individuals, Fig. 2). Fixed effects were mean-centered and standardized. Outputs include the estimated parameter value (± standard error) and a type-I likelihood ratio test to investigate the significance of each fixed effect sequentially. Fixed effects that were found to have a significant effect (p < 0.05) are bolded

(Table 1, Fig. 2E). The kinematics of large males did not permit them to compensate their weight by flying faster horizontally and significantly increased their negative vertical (i.e., sinking) speed (Additional file 1: Fig. S5, Table 1). Thus, large males were impaired in their agility and ability to climb.

Small males attach to substrates better than larger males, reducing their risk of falling

Safely attaching to leaves and branches with their tarsi is critical for canopy-dwelling leaf insects. Females spend most of their time hanging from the undersides of leaves and therefore rely on friction attachment forces, which resists tarsal movement along (parallel to) the surface of the leaf, and adhesion forces, which resists falling from the underside of the leaf (i.e., perpendicular to the leaf surface). Male attachment performance also depends on both friction and adhesion forces, but males walk greater distances through the canopy in their search for females, requiring them to attach to a wider variety of plant surfaces (e.g., leaves, branches, trunks), and flying males must overcome impact forces to hold on to branches or leaves when they land.

Friction (parallel to the substrate) and adhesion (perpendicular) forces are the product of maximum tarsal pad frictional or adhesive strength and pad area. Tarsi of male and female *P. philippinicum* are similar in overall morphology. Both sexes have five-segmented tarsi, each of the tarsomeres equipped with a euplantula (i.e., "heel" pads), and an arolium (i.e., "toe" pads) and two claws on

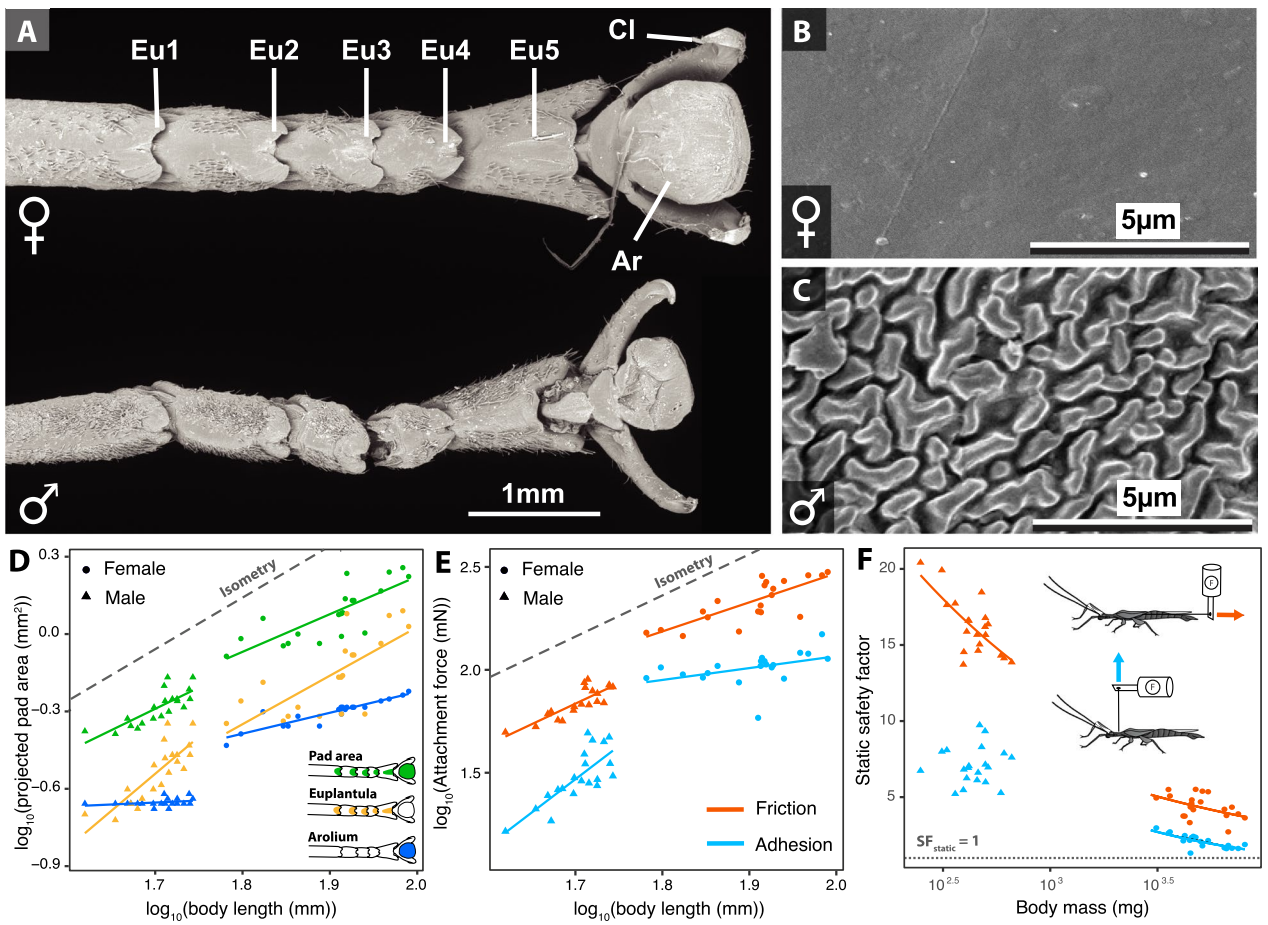

Fig. 3 Sexual dimorphism in tarsal morphology and attachment forces in *P. philippinicum*. **A** Morphology of female (top) and male (bottom) metathoracic tarsi. Eu. euplantula, Cl, claw, Ar, arolium. Euplantular attachment microstructures are smooth in females (**B**) and bear maze-like cuticular patterns in males (**C**). **D** Scaling relationships between body length and adhesive pad areas. **E** Friction and adhesion forces as a function of body length. Dots represent maximum force measurements averaged for each individual over three trials. Dashed lines in **D** and **E** represent the slope expected under isometry (slope = 2, arbitrary intercept). **F** Static safety factor as a function of body mass. The x-axis is on a $\log_{10}$ scale. The dotted line in (**F**) represent a safety factor of one. Diagrams represent the experimental set-up to measure friction (orange) and adhesion (blue) forces

the pretarsus (Fig. 3A), as is typical for phasmids [42, 43]. The primary region of tarsal friction is the euplantula, and for adhesion is the arolium [44]. The overall size of these tarsal pads scales isometrically with BL and does not differ between sexes after accounting for size differences (Table 2, Fig. 3D). However, scanning electron microscopy (SEM) revealed that the attachment microstructures on the euplantulae are sexually dimorphic. The euplantulae of females are smooth, without cuticular microstructures (Fig. 3B), while in males this surface is covered with maze-like arrangements of ridges (Fig. 3C; sensu [42, 43, 45]). These cuticular microstructures are likely to perform better, on average, on a broad range of substrate surfaces males experience from active searching. In contrast, smooth euplantulae are specifically adapted to smooth substrates such as the surface of smooth leaves [45, 46].

To test for effects of body size on attachment performance, we measured maximal tarsal friction and adhesion using a force transducer mounted on a motorized micromanipulator. Static safety factors (SF_{static}) were calculated from measures of the force required to pull the insect horizontally off a glass plate (friction forces), or backwards off the plate (adhesion forces), divided by weight (see "Materials and methods"). This approximates how many times leaf insects can attach their own weight to smooth canopy surfaces when they are resting or hanging motionless, which is what females do most of the time. Larger males displayed higher adhesion and friction attachment forces than smaller ones. This positive correlation between attachment force and BL was also found in females, but only when considering friction forces (Fig. 3E, Table 2). Females also had relatively higher adhesion and friction attachment forces than males (Fig. 3E, Table 2). However, females, with their large, leaf-mimicking bodies and mainly motionless behavior, had the lowest static safety factors (Fig. 3F, Table 2). As they were much lighter, males had relatively larger friction SF_{static} than females (Fig. 3F, Table 2), consistent with the greater attachment demands they experience from active searching and, especially, landing. While males displayed relatively higher adhesion SF_{static}, this difference was not significant ($p = 0.068$, Fig. 3F, Table 2). In females, adhesion and friction SF_{static} negatively correlated with body

Table 2 Scaling relationships between body size and attachment structures and forces

Response variable (log_{10} transformed)	Explanatory variables	F	df1	df2	p	Isometric slope	Slope β [95% CI]
Pad morphology							
Arolium area (mm^2)	**log_{10} (body length)**	**3460**	**1**	**36**	**< 0.001**	2	Males: 0.15 [− 0.07, 0.37] Females: 0.81 [0.63, 0.99]
	Sex	**245.2**	**1**	**36**	**< 0.001**		
	Interaction	**19.0**	**1**	**36**	**< 0.001**		
Euplantula area (mm^2)	**log_{10} (body length)**	**225.6**	**1**	**36**	**< 0.001**	2	Males: 2.86 [1.87, 3.86] Females: 1.88 [1.00, 2.77]
	Sex	0.42	1	36	0.52		
	Interaction	1.81	1	36	0.19		
Combined pad area (mm^2)	**log_{10} (body length)**	**483.0**	**1**	**36**	**< 0.001**	2	Males: 1.65 [1.01, 2.28] Females: 1.46 [0.90, 2.02]
	Sex	2.41	1	36	0.13		
	Interaction	0.17	1	36	0.68		
Attachment forces							
Adhesion forces (mN)	**log_{10} (body length)**	**444.4**	**1**	**36**	**< 0.001**	2	Males: 3.22 [1.93, 4.51] Females: 0.58 [− 0.03, 1.18]
	Sex	**24.3**	**1**	**36**	**< 0.001**		
	Interaction	**16.5**	**1**	**36**	**< 0.001**		
Friction forces (mN)	**log_{10} (body length)**	**803.4**	**1**	**36**	**< 0.001**	2	Males: 1.98 [1.34, 2.63] Females: 1.41 [0.86, 1.97]
	Sex	**18.3**	**1**	**36**	**< 0.001**		
	Interaction	1.54	1	36	0.22		
Static adhesion safety factor	**log_{10} (body mass)**	**562.2**	**1**	**36**	**< 0.001**	0	Males: 0.06 [− 0.3, 0.43] Females: − 0.58 [− 0.85, − 0.31]
	Sex	3.5	1	36	0.068		
	Interaction	**9.11**	**1**	**36**	**0.005**		
Static friction safety factor	**log_{10} (body mass)**	**980.9**	**1**	**36**	**< 0.001**	0	Males: − 0.34 [− 0.51, − 0.17] Females: − 0.33 [− 0.64, − 0.02]
	Sex	**5.31**	**1**	**36**	**0.027**		
	Interaction	0.008	1	36	0.93		

The table presents results of type I ANOVA from linear models contrasting the differences between sexes in terms of scaling relationships between body size and attachment pad areas, attachment forces and static safety factors (N = 20 males and 20 females, Fig. 3). Scaling exponents β and the corresponding 95% confidence intervals are shown in comparison to isometric expectations. Significant effects (i.e., $p < 0.05$) are bolded

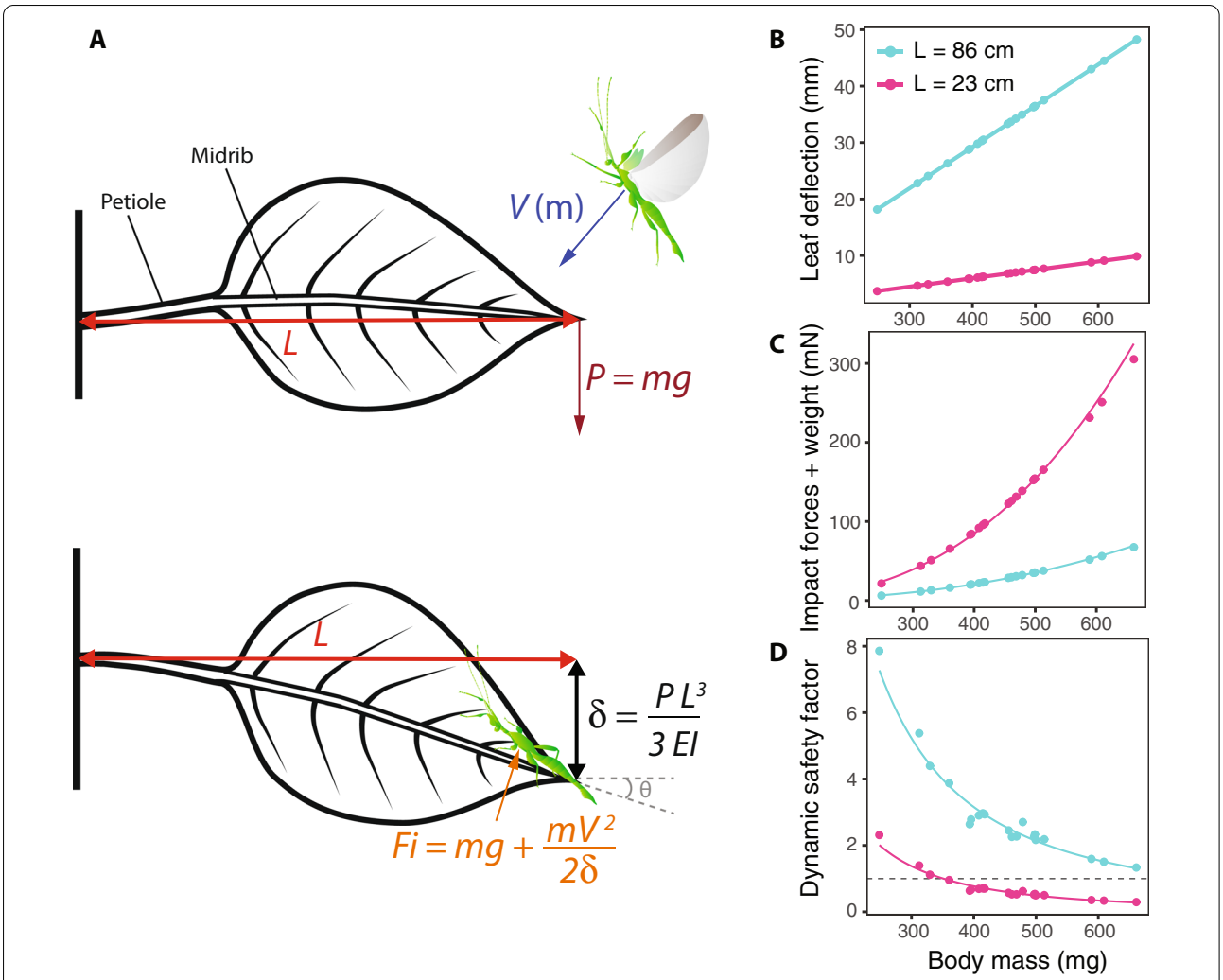

Fig. 4 Landing model calculations and predictions. **A** Diagram of a male leaf insect landing on a leaf, including calculations used to estimate impact forces (F_i) and dynamic safety factors ($SF_{dynamic}$)—i.e., the ratio of frictional attachment forces and F_i. The male lands with a landing velocity V which depends on the body mass of the insect (m). The terminal load on the leaf (P) will be equal to the weight of the insect—i.e., body mass (m) multiplied by the acceleration due to gravity (g). The subsequent deflection of the leaf (δ) depends on P, the length of the leaf (L) and the leaf flexural stiffness (EI). The impact force experienced by the male leaf insect (F_i) will be determined by P, the kinetic energy of the insect ($mV^2/2$) and δ. See the text for more detailed information. Predicted relationships between male body mass (m) and δ (**B**), F_i (**C**) and $SF_{dynamic}$ (**D**). Predictions for large leaves (L = 86 cm) are represented in blue, small leaves (L = 23 cm) in pink. The dashed line in (**D**) represents a safety factor of one

mass, while in males, only friction SF_{static} significantly decreased with increasing body mass (Fig. 3F, Table 2). Therefore, larger males are at higher risk of slipping off smooth substrates when resting or walking but the relatively high values of SF_{static} (> 14) question the ecological relevance of such decreased attachment capacity.

Flying males, in contrast to females, experience additional attachment demands when they land, due to impact forces. Consequently, to investigate the potential order of magnitude of these forces and how they may affect safety factors, we built a model to predict the typical impact forces experienced by males (F_i) when landing on a leaf. This model computed dynamic safety factors ($SF_{dynamic} = \frac{F_{friction}}{F_i + Body\ weight}$) based on landing speed and leaf deflection estimated from body mass. Landing platforms (i.e., leaves) were modelled as cantilever beams spanning a range of size and flexural stiffness (reused from other studies [47]) as, in the field, landing platforms encountered by flying males during mate search may display extremely variable mechanical properties. Our goal was to estimate potential extreme values of impact force. Only frictional attachment forces (as opposed to adhesive forces) were used to compute these $SF_{dynamic}$ as they are

the most important for accommodating deceleration and impact forces when landing [47].

Our landing model (Fig. 4A) predicted heavier males to cause larger leaf deflections when landing as estimated by Eq. 3 (Fig. 4A, B). Leaf deflection was greatest for the largest leaves (Fig. 4B). We empirically found, in our flight experiments, that overall landing velocity was positively correlated with male body mass (Additional file 1: Fig. S6, likelihood ratio test: $\chi^2 = 4.12$, df = 1, p = 0.042). This is due to heavier males dropping faster as horizontal velocity was not significantly correlated with body mass (Table 1). In our landing model, we then used the fixed effect estimates of the corresponding linear mixed model to predict the landing velocity of males given their body mass and estimate impact forces at landing (Fig. 4A). Landing impact forces were predicted to increase with male body mass and to be relatively higher for smaller leaves (Fig. 4C, Table 3). Finally, the model estimated that $SF_{dynamic}$ should decrease with male body mass and should be relatively lower for smaller leaves (Fig. 4D, Table 3). Interestingly, predicted $SF_{dynamic}$ fell below 1.0 for body masses > 350 mg and small leaves (Fig. 4D), therefore predicting slippage. In other words, large males were predicted to be more likely to slip and fall when landing on canopy substrates, especially on smaller and stiffer leaves.

Body shape affects lift:drag ratio

To further understand how body size and shape affect aerodynamics in ways that could contribute to flight performance, we generated 3D models of the bodies of males of varying size and abdominal shape and estimated body lift and drag during steady horizontal flight using computational fluid dynamics modelling (CFD, Fig. 6A, see "Materials and methods") [48–50]. Contrary to vertical velocity, mean horizontal velocity did not significantly correlate with body mass in our flight trials (Table 1). Therefore, the CFD simulations of horizontal flight were run at a constant average speed (1.57 m s^{-1}). The models predicted that the male's flattened abdomen would produce a wide region of low-pressure behind the insect, the size of which largely being dependent on its shape (Fig. 5). The males' poorly streamlined bodies would create high drag coefficients ($1.38 < C_D < 1.55$, Fig. 6C) and only nominal lift coefficients ($0.85 < C_L < 1.03$, Fig. 5D) resulting in relatively low lift to drag ratios ($0.56 < L/D < 0.74$, Fig. 6B).

Our simulations further suggested that flying males with wider abdomens generate more lift relative to drag, have a lower C_D, and a higher C_L (Fig. 6B–D, Table 4). In contrast, body size did not significantly affect these parameters (Table 4). The drag and lift forces applied by the air on the animal's body (expressed as proportion of body weight) were estimated to be higher in smaller males with wider bodies (Fig. 6E, Table 4). Interestingly, body lift and drag were predicted to decrease at similar rates with body aspect ratio, suggesting that the gain in body lift provided by wider bodies (i.e., helping in weight support) may be offset by the gain in body drag (i.e., opposing the movement). Thus, contrary to our predictions, our models suggest that abdominal shape may not significantly affect the cost of flight and that selection for flight efficiency may not explain the relatively slenderer body shape of males in this species.

The power required for flight increases with size faster than the available muscle power.

Flight performance depends on the power available (the maximum amount of mechanical energy that can be provided by the flight muscles per unit of time, P_a) and on the power required for flight (the amount of mechanical energy required to fly per unit of time, P_r) [51]. We theoretically estimated the scaling exponents of these two variables with BL using our empirical data to uncover how the difference between them (ΔP), which represents the excess power available for demanding aerial activities, varies with size. We estimated that P_a increases with body size with a scaling exponent $\beta_{P_a} = 2$, as expected under isometry.

Table 3 Tests of the effect of body mass and leaf size on estimated (modelled) landing impact forces and dynamic safety factors in males (N = 20 males, Fig. 4)

Response variable (log_{10} transformed)	Explanatory variables	F	df1	df2	p	Slope β [95% CI]
Impact forces + weight (mN)	log_{10}(body mass)	**20,541**	**1**	**36**	**< 0.001**	Small leaf: 2.67 [2.6, 2.74] Large leaf: 2.41 [2.38, 2.43]
	leaf size	**31,459**	**1**	**36**	**< 0.001**	
	interaction	**55.7**	**1**	**36**	**< 0.001**	
Dynamic friction safety factor	log_{10}(body mass)	**892**	**1**	**36**	**< 0.001**	Small leaf: − 2.02 [− 2.21, − 1.82] Large leaf: − 1.75 [− 1.92, − 1.57]
	leaf size	**2485**	**1**	**36**	**< 0.001**	
	interaction	**4.40**	**1**	**36**	**0.043**	

Type-I ANCOVAs were performed. Scaling exponents β and the corresponding 95% confidence intervals are shown for small and large leaves separately. Significant effects (i.e., p < 0.05) are bolded

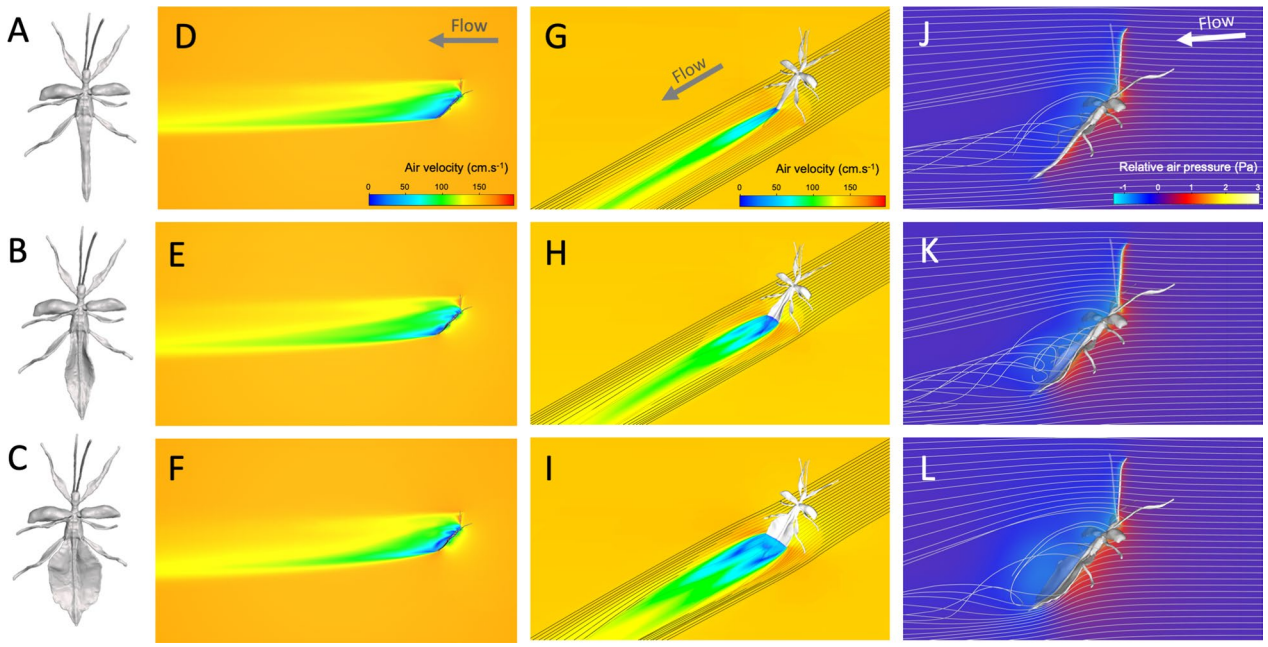

Fig. 5 3D models and computational fluid dynamics simulations. Dorsal view of phasmid models with no (**A**), natural (**B**) and widened (**C**) 'leaf-like' abdominal expansions. Air velocity in the mid-sagittal plane (**D**–**F**), air velocity and streamlines in a horizontal transverse plane (**G**–**I**), pressure (relative to ambient air static pressure) and streamlines in the mid-sagittal plane (**J**–**L**) around the bodies of males with no (**D**, **G**, **J**), natural (**E**, **H**, **K**) and widened (**F**, **I**, **L**) abdominal expansions

In contrast, P_r increases with body size with a scaling exponent $\beta_{P_r} = 5.5$ (95% CI [4, 7]) where isometry predicts $\beta = 3.5$ (Eq. 5). Consequently, ΔP ($P_a - P_r$) decreases with body size more rapidly than would be expected under isometry, hypothetically accounting for the reduced flight climbing ability and maneuverability seen in larger males. Combined, our results suggest that selection for both flight and landing/attachment performance may help explain the relatively small size of males in this species.

Discussion

As leaf masqueraders, leaf insects (Phylliidae) display some of the most extreme abdominal morphologies of the insect world, and sexual size and shape dimorphisms so spectacular that taxonomists have had difficulty associating males and females of the same species [32]. Using these organisms, we provide support for the hypothesis that selection for locomotor performance favors small body sizes in males, contributing to the evolution of extreme sexual dimorphism in insects with scramble competition mating systems.

We show that small males have greater agility in the air, as they were able to stabilize their body angle faster after falling [40], and they were better able to climb in flight than larger males. Flight is most likely essential to the mate searching performance of males, as females are sedentary and typically scattered in the rainforest canopy [14]. A decreased agility in the air and a lower ability to maintain a horizontal trajectory or ascend during flight may be detrimental in that regard. It should however be noted that pitch control is only one aspect of maneuvering; roll and yaw likely also contribute [52]. Our momentum-jet analysis suggested that the mechanical power required for these males to fly steadily and horizontally (P_r) should increase at a faster rate than the power available from the flight muscles (P_a), and even faster than expected under isometry. The reduction of flight performance (agility and climb ability) with body size seen in leaf insects is therefore likely to result from the decrease of ΔP ($= P_a - P_r$), which represents the excess power available for more demanding aerial activities such as maneuvers and climbing in air [51, 53].

Not only were large males relatively poor flyers, they also were more likely to detach and fall from smooth substrates. Our measurements of attachment forces showed that static safety factors for friction forces decreased with body size in males but remained high (> 14), questioning the ecological relevance of this decrease. However, the attachment capacity of males is likely to get challenged at the landing, during which friction forces are fundamental to accommodate impact forces [47]. Our landing model predicted that the dynamic safety factors of the largest males were likely to come close or

Table 4 The effects of body size and shape on various aerodynamic variables, as predicted by the CFD models

Response variable	Explanatory variables	β ± SE	F	df1	df2	p
Lift to drag ratio (L/D)	Body length	0.001 ± 0.0007	2.72	1	22	0.11
	Body aspect ratio	**− 0.02 ± 0.001**	**221.7**	**1**	**22**	**< 0.001**
Drag coefficient (C_D)	Body length	− 0.001 ± 0.0008	2.42	1	22	0.13
	Body aspect ratio	**0.015 ± 0.001**	**103.1**	**1**	**22**	**< 0.001**
Lift coefficient (C_L)	Body length	0.001 ± 0.001	0.60	1	22	0.45
	Body aspect ratio	**− 0.02 ± 0.002**	**68.3**	**1**	**22**	**< 0.001**
Relative drag	**$\log_{10}$ (body length)**	**− 0.499 ± 0.049**	**103.0**	**1**	**22**	**< 0.001**
	$\log_{10}$ (body aspect ratio)	**− 1.058 ± 0.092**	**131.5**	**1**	**22**	**< 0.001**
Relative lift	**$\log_{10}$ (body length)**	**− 0.295 ± 0.055**	**28.6**	**1**	**22**	**< 0.001**
	$\log_{10}$ (body aspect ratio)	**− 1.245 ± 0.104**	**144.6**	**1**	**22**	**< 0.001**

Results of type I ANOVA from linear models contrasting the effects of body length and body aspect ratio on various aerodynamic variables (Fig. 6). Significant effects (i.e., $p < 0.05$) are bolded

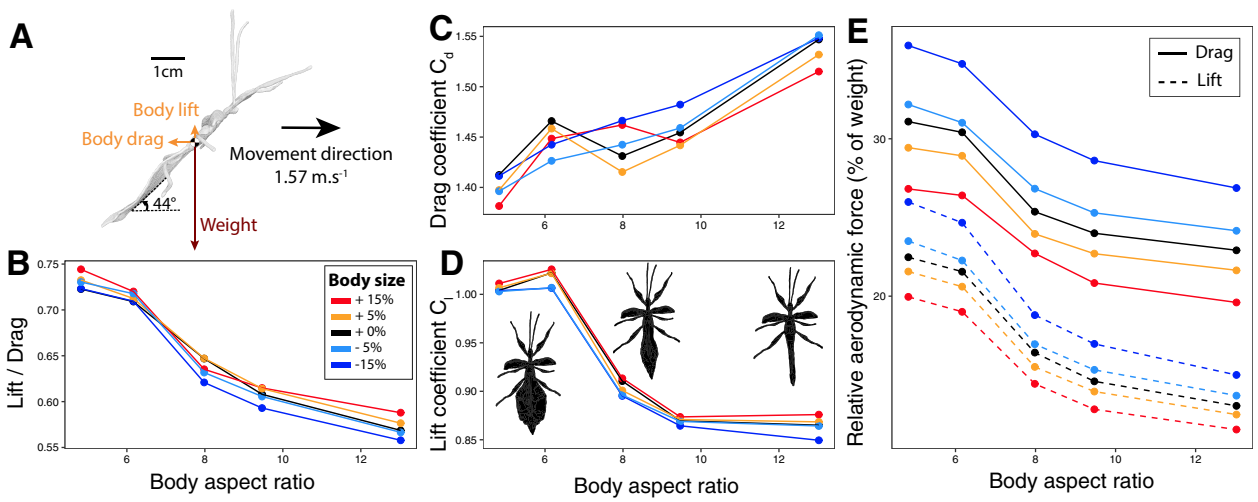

Fig. 6 The effects of body shape on body aerodynamics as predicted by computational fluid dynamics simulations. **A** Diagram of the forces applying upon the modelled flying male leaf insect. Lift to drag ratio (**B**), drag (**C**) and lift (**D**) coefficients, drag (**E**, solid) and lift (**E**, dashed) forces relative to body weight as a function of model aspect ratio as estimated from the CFD simulations. Colors correspond to different body sizes relative to the original model

even below one (i.e., slippage) when landing on small and stiff leaves. However, it should be noted that the material properties of the landing platforms encountered by males in the field are still unknown. Therefore, the significance of the decreased attachment performance of large males, remains to be tested in the field. High attachment safety factors are crucial for canopy insects to avoid falling, which can lead to predator exposure [54–56] and energetic costs to return to the canopy [34]. For searching males, it can also mean losing track of a female. We found that male leaf insects have specialized, ridged surfaces on the pads of their tarsi which are not present in females (Fig. 2B, C), and which are probably adapted to gripping a broad range of plant surfaces [45, 46, 57–60]. Flying males are likely to be confronted with unpredictable surfaces (e.g., branches, leaves) when walking and landing, and may benefit from generalist tarsal pads that adhere securely to a range of textured surfaces. In contrast, females move very little in the canopy and are strongly associated with the leaves of their food plants. Females likely use their claws and attachment pads on a narrower range of surfaces and for a narrower range of tasks—primarily as anchors as they hang upside down from smooth leaf cuticle. In this context, adhesion (as opposed to friction) forces are essential. In stick insects, arolia are shear-sensitive attachment pads providing most of the adhesion [44, 45]. Consistently, female leaf insects have larger arolia relative to body size than males and consequently produce larger adhesion forces. Nevertheless, as females weigh much more than males,

their static safety factors for both adhesion and friction forces were still relatively lower than those of males.

Male and female leaf insects also exhibit a spectacular interspecific variation in body shape related to leaf mimicry [24, 26, 61]. This variation is likely driven by masquerade and the advergence of the insect appearance to resemble the size and shape of its host plants' leaves. Thus, predation is likely a major selective agent acting on male and female morphology that may greatly constrain or even oppose selection on male morphology imposed by locomotion, notably selection favoring smaller body sizes. As exemplified by *P. philippinicum*, flight-capable males have more elongated body shapes than their respective flightless females and relatively reduced abdominal leaf-like lobes. Our CFD models coupled with scaling of body weight predicted that despite the poorly streamlined body shapes of males and their high drag coefficients ($C_D > 1$), any increases in body drag due to wider body shapes would be offset by increased body lift. This leads us to predict a similar net cost of flight for thin or wide males. Therefore, flight performance may not constrain male body shape the way that it does body size, and may have provided male leaf insects the freedom to evolve a variety of body shapes [62–66]. However, given that body shape still significantly affected the aerodynamic forces applying on the insect body, it is possible that it affects other relevant components of aerial performance beyond the scope of this study such as maneuverability and stability, or the net cost of flight in other contexts like ascending flight.

Our empirical and modelling approaches were designed to test how different aspects of leaf insect locomotor performance scaled with body size and shape in multiple relevant contexts. However, our models included a number of simplifying assumptions which we acknowledge, and future studies may wish to expand their focus accordingly. For instance, we chose a constant and average leg posture, flight direction (horizontal), flight speed and angle of attack in our CFD models, and we ignored the complexity of wing aerodynamics, all of which are likely relevant to the aerodynamic of the insect in flight. Similarly, our estimates of impact forces at landing are simplified as, for example, we did not account for the leg joint movement that may further reduce the impact force. More detailed modelling approaches and empirical tests of the predictions from our models (e.g., by measuring aerodynamic forces and slippage probability when landing) are worthwhile goals for future, more specific, studies.

Conclusions

In summary, our analyses suggest that large scrambling males are at a locomotor disadvantage in at least two aspects of mate searching in leaf insects: they have lower agility and ascending flight abilities likely stemming from lower power margins to fly, and they are at a higher risk of falling when landing on surfaces in search of rare and scattered females. Therefore we offer support for the hypothesis that large scrambling males suffer multiple locomotor costs in several critical aspects of mate searching. Our findings help to shed light on the repeated evolution of relatively small males in scramble competition mating systems by explicitly considering locomotor performance as an intermediate step between morphology and mobility and mating success.

Materials and methods

Study animals

A first breeding population of *P. philippinicum* was obtained from the Audubon Insectarium in New Orleans, Louisiana, USA and shipped to the University of Montana, Missoula, Montana, USA. The insects were housed in a transparent plastic container ($50 \times 40 \times 60$ cm) at 22 °C, on 12 h:12 h light:dark cycles, sprayed with water daily (RH = 50–80%), and fed fresh *Rubus idaeus* leaves ad libitum. This population was used to investigate morphological scaling relationships and conduct the flight experiments described below.

A second culture stock of *P. philippinicum* was obtained from Kirsten Weibert (Jena, Germany) and captive bred in the department of Functional Morphology and Biomechanics at Kiel University, Germany. The specimens were kept in a large glass cage with proper ventilation at 20–22 °C (RH = 50–80%; 16 h:8 h light:dark cycle) and fed with fresh blackberry (*Rubus* sp.) and common oak (*Quercus robur* L.) leaves ad libitum. This population was used to investigate attachment pad morphology and attachment forces.

Sexual dimorphism and scaling relationships

Photographs of the animals in dorsal view were taken using a DSLR camera (EOS 600D, Canon Inc., Tokyo, Japan). Using ImageJ software (v.1.52k) [67], we measured body length (BL, mm), body area (mm^2), body circularity (dimensionless, $\frac{4\pi \times Area}{Perimeter^2}$), body aspect ratio (dimensionless, $\frac{Body\ length}{Average\ body\ width}$), mean antenna length (mm), mean front femur length (mm), and total wing area (mm^2, including both forewings for females or both hindwings for males) in 25 adult males and 19 adult females (Additional file 1: Fig. S1). Antenna length could not be measured in seven males and three females because they were missing flagellomeres on both antennae. Wet body mass (g, measured immediately after flight trials) was obtained using an analytical balance (ME54TE/00, Mettler Toledo, Columbus, OH, USA). We calculated wing loading ($N\ m^{-2}$) as wet body mass multiplied by gravitational acceleration ($g = 9.81\ m\ s^{-2}$) and

divided by total wing area. Male flight muscle mass (mg) was obtained by dissecting the muscles out of the metathorax of freshly dead males (n = 23) drying them at 70 °C for 24 h and weighing them with a more accurate analytical balance (UMT2, Mettler Toledo, Columbus, OH, USA).

Male flight performance

To evaluate male flight performance, here defined as a righting maneuver that required sustained control over long-axis body angle and climb ability, we dropped adult males in the air and recorded their flight trajectories in 2D (Additional file 2: Video S1, Additional file 3: Video S2). Working in Missoula, MT (elevation 978 m above sea level, average air density = 1.07 kg m^{-3}), adult males (N = 16, 0.43 ± 0.006 g) from our American culture population were held by the thorax and dropped by the experimenter at a horizontal body angle from a constant height above a floor (1.5 m). A 2 m-tall slab of ponderosa pine (*Pinus ponderosa*) with natural bark was placed vertically in front of the animal, 2 m away, to serve as a target and landing site (Additional file 1: Fig. S3). The experimental room was largely featureless with white walls and at 26 °C. The floor was covered with thick blankets to avoid injuries if crashing. We recorded the flight of the insects using a high-speed video camera (Photron FASTCAM SA-3, Photron USA, San Diego, CA, USA) sampling at 500 fps with a shutter speed of 1/5000 s and 1024 × 1024 pixel resolution (Photron PFV v.3.20). Because the insects were induced to fly in a trajectory parallel to the plane of the imaging sensor (deviations < 10°), we analyzed the trajectories in two dimensions (Additional file 1: Figs. S3, S4A). Pixels were scaled to metric coordinates using a 50 cm bar held horizontally at the same level of the flight trajectories. We recorded a clay ball in free fall to calibrate the vertical direction. Average vertical ball acceleration was 9.816 ± 0.14 m s^{-2}, less than 1% different from gravitational acceleration (9.805 m s^{-2}) and the camera was oriented to gravity so that the vertical ball drop direction of acceleration was always < 5% of 90°. Each insect was dropped several times (maximum five times) until we obtained two straight trajectories per animal. A resting period of approximately 20 min was left in between each flight to allow recovery. Males were frozen-killed at − 80 °C just after the experiments. After estimating the relative position of their center of mass (see below), males were pinned with their wings fully extended for morphometrics.

Video digitization was done by tracking morphological landmarks using the open source video analysis tool *DLTdv5* by T. Hedrick implemented in MATLAB (R2016b, MathWorks, Natick, MA, USA) [68] and the obtained data was analyzed using R (v 3.6.1) [69]. In *DLTdv5*, we used autotracking mode (predictor tool: extended Kalman) and manual tracking when the autotracking mode was unreliable. We marked the position of the head and of the terminal abdominal segment on each frame. Body pitch (°) was calculated for every frame by calculating the angle between the horizontal and the line linking the position of the head and that of the terminal segment (Additional file 1: Fig. S4B). Typically, in the first phase of the fall (free fall), body pitch decreases (i.e., the insect rotates forward, eventually diving head first), before the insect opens its wings (t_1) and actively corrects (t_2) and stabilizes its body pitch (phase 3) (Additional file 1: Fig. S4B). Body pitch was smoothed using a Savitzky–Golay filter with a polynomial order of 3 and a window size of 71 (*sgolayfilt*: 'signal', *function*: 'R package'). The beginning of phase 2 (t_1) was determined as the time corresponding to the minimal body pitch (Additional file 1: Fig. S4B). The end of phase 2 (t_2) corresponded to the time when the insect's pitch stabilized—i.e., when the rotational velocity (° s^{-1}) of body pitch reached a local minimum after a large peak corresponding to phase 2 (Additional file 1: Fig. S4B). We calculated the average rotational velocity during phase 2 (ω) as:

$$\omega = \frac{Body\,pitch(t_2) - Body\,pitch(t_1)}{t_2 - t_1} \quad (1)$$

We used ω to quantify torsional agility—an important aspect of maneuverability—as it reflects how fast the animal can rotate to correct its body pitch in the air from a free falling, head first, position to a stable flight body pitch. This correction occurred over several wingbeats and was therefore distinct from within and among-wingbeat oscillations which could have indicated a lack of longitudinal stability [41]. The 2D position of the body center of mass was estimated using images taken in lateral view of the males (freshly dead) orthogonally balancing on a horizontal razorblade. Its position relative to the two landmarks (i.e., head and terminal segment) was then calculated which enabled us to define the center of mass of the individual on each flight video. Trajectories of the center of mass were analyzed using the package "trajr" in R [70]. Raw trajectories were smoothed using a Savitzky–Golay filter with a polynomial order of 3 and a window size of 31 (*TrajSmoothSG*: 'trajr'; Additional file 1: Fig. S4A). Horizontal, vertical and composite velocities and accelerations were then computed on the smoothed trajectories (*TrajDerivatives*: 'trajr'; Additional file 1: Fig. S4C, E). For each trial, we defined transient and steady states for both vertical and horizontal velocities (Additional file 1: Fig. S4D, E). In both cases, the transient state corresponded to the free fall and maneuver of the insect in the air during which body velocity greatly varied. The steady state started when velocity stabilized and acceleration started oscillating around 0 m s^{-2} (Additional file 1:

Fig. S4D, E). We extracted the mean vertical and horizontal velocity (m s^{-1}) during their respective steady states. These measures were used to quantify the capacity of the insect to fly forward and ascend. On the videos, the position of the tip of the wing closest to the camera was also manually marked on frames corresponding to the end of upstroke and downstroke as this was sufficient to measure wing beat frequency (Hz) and stroke amplitude (°). Average wing beat frequency was calculated after the animal reached a stable body pitch (i.e., after t_2; Additional file 1: Fig. S4B). For each animal, we measured wing length and the position of the attachment of the wings relative to the head and tip of the abdomen using photographs and ImageJ. We then determined the position of the wing attachment point on each frame on the videos using this relative position between our two landmarks. The amplitude of wing strokes was calculated using trigonometry (Additional file 1: Fig. S7).

Adhesive pads and substrate attachment performance

We used scanning electron microscopy (SEM) to observe the tarsi of the metathoracic leg of adult males and females, measure attachment pad areas, and describe the microstructures on these pads. Tarsi of the right metathoracic leg were cut off from 20 adult males and 20 adult females and fixed in 2.5% glutaraldehyde in PBS buffer for 24 h on ice on a shaker, dried in an ascending alcohol series, critical-point dried and sputter-coated with a 10 nm layer of gold–palladium. To obtain overview images, we used a rotatable specimen holder [71] and the scanning electron microscope (SEM) Hitachi TM3000 (Hitachi High-technologies Corp., Tokyo, Japan). The micrographs for visualization and measurements were taken at an acceleration voltage of 15 kV. The attachment microstructures on the tarsi of both sexes were further examined using the SEM Hitachi S4800 (Hitachi High-Technologies Corp., Tokyo, Japan) at 7 kV of acceleration voltage. Processing of the raw micrographs and measurements of projected attachment pad area (mm^2)—i.e., the surface area of the tarsus specialized for adhesion and friction [72, 73]—were done using Photoshop CS6 (Adobe Systems Inc., San José, CA, USA).

To measure attachment forces (mN) in both pull-off (adhesion) and traction (friction) directions, we used 20 adult males (Mean ± S.D. = 0.46 ± 0.02 g) and 20 adult females (5.22 ± 0.31 g). A horsehair was glued to the metanotum of each insect and then attached to a 100 g force transducer (FORT100, World Precision Instruments, Sarasota, USA, linearity error: < 0.1%, resolution: 0.01%), connected to a BIOPAC model MP100 and TCI-102 system (BIOPAC Systems, Inc., Goleta, CA, USA), and mounted on a motorized micromanipulator (DC 3001R, World Precision Instruments Inc.). Maximum adhesion forces were recorded by vertically pulling the insects off a horizontal glass plate until they detached from the glass plate [45, 74]. The micromanipulator was moved upwards with a speed of 200 µm/s at a step size of 10 µm until the specimen was detached from the surface as indicated by an instantaneous drop in force. Maximum friction forces were recorded by horizontally pulling the insects backwards with the same retraction velocities as above, until detaching them from the glass plate [45, 75]. A glass plate was used as the substrate for the attachment force measurements, to eliminate mechanical interlocking of the claws with surface irregularities of rough substrates, or penetration of soft substrates. As glass is smooth on the microscopical level, this substrate enables estimation of the traction and pull-off performance of the attachment pads themselves on a standardized level, without the influence of substrate irregularities. Force–time curves were obtained using Acqknowledge 3.7.0 (BIOPAC Systems Inc., Goleta, CA, USA) and the maximum peaks were extracted as maximum adhesion forces, or maximum friction forces respectively. Each of the 20 males and females were measured three times in both directions on a glass plate and the average of the three measurements was used as the individual maximum adhesion/friction force. The order of the individuals was randomized and the substrate was cleaned between every measurement. The experiments were conducted at 20–23 °C and 50–60% relative humidity.

Static safety factors (i.e., $SF_{static} = \frac{Attachment\ force}{Body\ weight}$) were computed for each individual. Following the methods of Higham et al., 2017 [47], we estimated impact forces (F_i, in N) during landing using a model to eventually compute dynamic safety factors (i.e., $SF_{dynamic} = \frac{Friction\ force}{F_i}$). In our landing model, we assumed that males would stop immediately after landing on the tip of a leaf without slippage. F_i was calculated using the work-energy principle:

$$F_i = mg + \frac{mv^2}{2\delta} \tag{2}$$

where m = mass of the insect (kg), g = acceleration of gravity (9.81 m s^{-2}), v = landing speed of the insect (m s^{-1}) and δ = deflection of the leaf (m) (Fig. 4).

We used a simplified model of a leaf to estimate a range of values for the deflection of a leaf upon landing of a male leaf insect and explore potential values of $SF_{dynamic}$. The leaf and petiole were considered as a uniform cantilever beam with impact forces applying at the tip at length L. We considered the leaf to be initially horizontal. Deflection was calculated as a function of the weight of the insect. Given the relatively light

weight of male leaf insects, and in contrast with [47], who were considering geckos (i.e., roughly 28 times heavier), we only accounted for small leaf deflections (deflection angle $\theta < 5°$) and therefore used the following equation to estimate the deflection of the tip of the leaf δ [76]:

$$\delta = \frac{mg\,L^3}{3EI} \quad (3)$$

where L is the total length of the leaf (m) and EI is its flexural stiffness (N m^2). We used the range of values estimated by [47], for leaf length and corresponding EI (i.e., $L_1 = 23$ cm, $EI_1 = 2.67 \times 10^{-3}$ N m^2 and $L_2 = 86$ cm, $EI_2 = 28.48 \times 10^{-3}$ N m^2) to account for the diversity of leaf mechanical properties and thus explore the possible range of $SF_{dynamic}$.

Finally, landing speed was estimated as a function of the body mass of the individual. Using our experimental flight videos (see above), we extracted the instantaneous speed of the experimental males right before making contact with the wood slab (i.e., the landing target) and built a linear regression between landing speed and body mass, including individual ID as a random factor (*lmer*: 'lme4', [77]). We found a significant positive effect of body mass on landing speed (see "Results", Additional file 1: Fig. S6) and used the fixed-effect estimates (intercept and slope) from this model to predict the landing speed of the males for which we empirically measured attachment forces, given their body mass. This estimated landing speed was used in Eq. 2.

Computational fluid dynamic simulations

To investigate how lift and drag produced by the insect were affected by size and shape, we generated 3D models of males of varying size and shape and predicted these forces during a steady and horizontal flight using computational fluid dynamics (CFD). We created a reference 3D surface model of an adult male body using photogrammetry. We pinned the body of a dead specimen in a flight posture (i.e., legs extended, forewings opened perpendicularly, antennae oriented 50° up, hindwings removed). We did not model flapping aerodynamics as fully integrating the complex three dimensional trajectories and aeroelastic deformations of the wings into a CFD model (e.g., [78]) was beyond the scope of this study. The aerodynamic interactions of the flapping wings with the body of insects in slow flight has been shown to be negligible (~5%) in [79]. Once dried, the individual was vertically mounted onto a pin on a custom-made turntable. 2D images using a DSLR camera (EOS 600D, Canon Inc., Tokyo, Japan) equipped with a macro lens (Canon EF 100 mm f/2.8 Macro USM), were then obtained from 100 different orientations (Additional file 1: Fig. S8). The 3D model was then reconstructed from these multiple images using Autodesk ReCap Pro 2019 (v5.0.4.17, Autodesk Inc., San Rafael, CA, USA) and subsequently smoothed and rewrapped using Autodesk Meshmixer 2017 (v11.5.474, Solid accuracy: 402, cell size: 0.202, density: 219, offset: 0.25, min thickness: 0.14 mm). From this reference model, we built four additional and artificial models using the "Move" tool in Meshmixer to either manually extend or shrink the abdominal lobes and therefore manipulate abdominal shape. These artificial shapes purposely spanned a wider range of body aspect ratios than the one found in actual males *P. philippinicum* (male natural range: 4.89–6.42, female natural range: 2.28–2.84, model range: 2.28–9.47). The model with the lowest aspect ratio displayed a female-like abdominal shape while the model with the highest aspect ratio had no abdominal expansions. The models were further scaled to a body length of 53 mm (mean male BL in our Montana population = 52.6 ± 0.25 mm) using Autodesk fusion 360 (v2.0.8335). From each of these five meshes, we created four additional models (25 models in total) respectively scaled to a factor 0.85, 0.95, 1.05 and 1.15. The insect models were tilted at a 44° body pitch in our control volume. This angle was determined using our flight experiments and a LMM with stable body pitch as the response variable, horizontal and vertical body velocity as main effects and individual ID as a random factor. Using the parameters estimated by this model, we predicted a body pitch of 43.9° for a vertical velocity of zero and a mean horizontal velocity of 1.57 m s^{-1} (i.e., the average horizontal velocity calculated from our flight trials, after the animal had stabilized its body pitch: 157 ± 6.8 cm s^{-1}).

We constructed a control volume around these body meshes in Autodesk CFD 2019 (v19.2), that provided numerical solutions to the Reynolds-averaged Navier–Stokes equations [50, 80]. A fluid volume was built around the mesh with walls far enough from the model mesh to avoid any reflection effects (1 × 0.5 × 0.5 m) (Additional file 1: Fig. S9A). The fluid was assigned the default properties of air in CFD 2019 (density at sea level = 1.205 kg m^{-3}, viscosity at 20 °C = 18.2 µPa s^{-1}). The phasmid models were then assigned properties of hardwood which, for mass-less and stationary models, should have no impact on results. The input flow on the anterior end of the control volume was set to 1.57 m s^{-1}. We held the air velocity around in the insect constant as we were only considering horizontal flight and average horizontal velocity after reaching a steady state did not significantly increase with size in our flight trials (Table 1, Additional file 1: Fig. S5A). We applied a zero-pressure condition on the opposing end of the volume. A slip/symmetry condition was applied to all other fluid boundaries. We automatically

meshed the domain around the phasmid model, applied a surface refinement, and locally defined a non-uniform mesh refinement region ($0.7 \times 0.2 \times 0.2$ m) with a mesh size reduced to 75%, around and behind the model to better capture the resulting wake. We ran steady-state simulations using the turbulence model k-epsilon. The maximum number of iterations was set to 3000 although the simulations were stopped when they reached convergence according to the default convergence detection parameters of the CFD software (mean = 849 ± 50 interactions). The adaptive meshing tool was used to insure mesh optimization for our models and mesh independence of the results. The simulation was first run with the meshing parameters described previously. Then, the solution results of this simulation were automatically used to refine the mesh in high velocity gradient regions and rerun the simulation. We enabled the 'flow angularity' option to improve mesh resolution in areas with a lot of flow separation, the 'free shear layers' and 'external flow' options to refine the mesh in areas of strong velocity gradients. We ran three such cycles for each model. Final mesh sizes averaged 865,446 ± 74,771 nodes and 4,411,596 ± 379,780 elements (Additional file 1: Fig. S9). Finally, to help evaluate the validity of our simulations, we placed a sphere with the same Reynold's number as the one calculated for the original phasmid model (Re = 5558) in a similar control volume with the exact same settings as our insect simulations. We found a drag coefficient (C_d) of 0.643. This is very close to the value predicted from experimental data ($C_d = 0.652$) and which was determined using the Eq. 8.83 in Morrison, 2013 [81].

The weight of the models (mN) with a non-modified abdominal shape (reference models) was determined from their BL using the linear regression built between male body mass and BL in our American population. To estimate the weight of the models with artificial abdominal shapes, we first measured their abdominal area relative to that of the reference model of identical BL and measured the average weight of the leaf-like abdominal expansions by cutting these extensions from five freshly frozen-killed males and measuring their areas and mass (89.7 ± 0.6 g m^{-2}). The CFD simulations estimated the aerodynamic forces (drag and lift, mN) that apply to the rigid insect body flying horizontally and steadily.

For each model, we measured the projected frontal area on a plane perpendicular to the air flow. We then calculated their coefficient of drag ($C_D = \frac{2F_{drag}}{\rho v^2 A}$) and lift ($C_L = \frac{2F_{lift}}{\rho v^2 A}$) using the model frontal area (A), the mass density of air (= 1.20473 kg m^{-3}), the velocity of the insect (v = 1.57 m s^{-1}) and the drag or lift force estimated from the CFD simulations. Lift to drag ratios ($\frac{C_L}{C_D}$) were also calculated for each model.

Scaling of muscle power available and power required for flight

From theory, we estimated the scaling relationships of the power available (P_a) and the power required for flight (P_r) with body size using our empirical data. As leaf insects are slow flyers (average flight speed = 1.70 ± 0.07 m s^{-1}, mean ± SE), P_r mostly corresponds to the induced power P_{ind}—i.e., the cost for producing lift [20, 51]. P_{ind} is the product of the net required force from the wings to maintain the animal in the air and of the induced velocity in the wake. Following [82], we assumed that, under isometry, the induced velocity in the wake and weight-specific power required for slow flight should be proportional to the square root of wing disc loading (DL, N m^{-2})—i.e., body weight (W_B) divided by wing disc area (A_{WD}). Wing disc area—i.e., the area swept out by the wing during a wing beat cycle and through which air is accelerated downward to develop lift force—is determined by wing length (L_w) and stroke amplitude (θ, °) (Eq. 4).

$$DL = \frac{W_B}{A_{WD}} = \frac{W_B}{2\pi {L_w}^2 \frac{\theta}{360}} \tag{4}$$

Thus, among geometrically similar animals, the power required for slow flight should scale as BL$^{7/2}$ (Eq. 5).

$$P_r \propto W_B (DL)^{1/2} \propto W_B \left(\frac{W_B}{2\pi {L_w}^2 \frac{\theta}{360}} \right)^{1/2} \propto BL^3 \left(\frac{BL^3}{BL^2} \right)^{1/2} \propto BL^{7/2} \tag{5}$$

In slow flight, P_a is the product of the net wing force and of the tangential velocity of the tip of the wing—i.e., angular velocity (rad s^{-1}) × wing length (m)—or the product of the muscle work—i.e., force × distance of contraction—and of flapping frequency (Hz). We accepted the assumption that, for geometrically and dynamically similar organisms, force is proportional to the cross-sectional area of the muscles, which scales as BL^2, and distance of contraction scales as BL^1. Thus, work scales as BL^3 and is therefore directly proportional to W_B [51, 83]. Flapping frequency is predicted to scale as BL^{-1} when the animal is using maximal or near-maximal effort [84]. Therefore, under isometry, P_a is expected to scale as BL^2.

To estimate the scaling exponent of the tangential velocity of the tip of the wing (i.e., angular velocity (rad s^{-1}) × wing length (m)) and of wing disc loading (Eq. 4) with L in leaf insects, we built LMMs with $\log_{10}$ tangential velocity or $\log_{10}$ disc loading as the response variable, $\log_{10}$ BL as the fixed effect and male ID as a random factor. Tangential velocity of the tip of the wing did not significantly scale with BL or differ from isometrical expectations ($\beta = -1$) in our flight experiments ($\beta = -2.43 \pm 1.60$, $\chi^2 = 2.46$, df = 1, p = 0.12). Similarly, the observed scaling exponents of body and flight muscle

mass did not significantly differ from isometric expectations (Additional file 1: Table S1). Coupling this with the aforementioned assumptions about muscle force, we estimated P_a scaled isometrically in leaf insects ($\beta = 2$). Wing disc loading (DL) positively scaled with BL ($\chi^2 = 8.99$, $df = 1$, $p = 0.003$). While, under isometry, we expected a scaling exponent of 1 (Eq. 4), we found that DL increased disproportionately with BL ($\beta = 4.96$, 95% CI [1.99, 7.94]). This is a consequence of the reduced wing stroke amplitude seen in larger individuals (Table 2). As the induced velocity (V_i) in the wake scales proportionately with the square root of wing disc loading, we estimated that P_r scaled more steeply with size than expected under isometry ($\beta = 5.48$ vs 3.5) (Eq. 6)

$$P_r \propto W_B(DL)^{1/2} \propto BL^3(BL^{4.96})^{1/2} \propto BL^{5.48} \quad (6)$$

Consequently, ΔP ($P_a - P_r$) decreased with body size more rapidly than would be expected under isometry.

Statistical analyses

All statistical analyses were run in R version 3.6.1 [69] and all statistical tests were two-sided. For all linear models, we systematically checked the normal distribution of the residuals and the absence of any specific patterns in their distribution.

We tested for sex differences in mean BL, body mass, body aspect ratio and antenna length using Wilcoxon–Mann–Whitney tests (*wilcox.test*: 'stats'). To test for sex differences in the scaling relationships (i.e., in slope and intercept) of the various morphological traits, attachment and aerodynamic force measurements with BL, we built ordinary least square regressions [85] including each $\log_{10}$-transformed trait as response variable and $\log_{10}$ BL, sex and their interaction as predictor variables (*lm*: 'stats'). Type-I ANCOVAs were used to determine significance of the fixed effects (*anova*: 'stats'). Departure from isometry which corresponds, on a log–log scale, to a slope of 1 for linear measurements, 2 for areas and 3 for masses [86], was tested using 95% confidence intervals (CI) around the estimated regression slopes (*confint*: 'stats'). We similarly built linear models to investigate the effect of body mass, leaf size (i.e., small or large) and their interaction on the estimated landing impact forces in males and dynamic safety factors.

To test for effects of body size, wing size and body shape on male flight performance, we built linear mixed models (LMM) (*lmer*: 'lme4'). Response variables were either rotational velocity (ω), mean vertical or horizontal velocity, wingbeat frequency, or wing stroke amplitude. Body mass, wing area and body aspect ratio were mean-centered and standardized ($\mu = 0$ and $\sigma = 1$, *scale*: 'base') and were included as main fixed effects. Individual ID was included as a random factor to account for replications of each individual. Likelihood ratio tests were subsequently performed sequentially to assess the significance of the fixed effects (*anova*: 'lme4'). For response variables significantly affected by body mass and wing area and to illustrate their combined effect, we built and plotted similar LMMs but with wing loading as the only fixed effect.

Following our CFD simulations, we tested for the effects of body size and shape on lift to drag ratio, C_D, C_L, and relative aerodynamic forces applying on the body using linear models including BL and body aspect ratio as explanatory variables. Sequential ANOVAs (type I) were subsequently performed to assess significance (*anova*: 'stats'). In models including relative force estimates as response variables, variables were $\log_{10}$-transformed to compute scaling exponents [86].

Abbreviations

SSD: Sexual size dimorphism; BL: Body length; ω: Body pitch rotational velocity; SEM: Scanning electron microscopy; SF_{static}: Static safety factors; F_i: Impact forces; $SF_{dynamic}$: Dynamic safety factors; CFD: Computational fluid dynamics; C_D: Drag coefficient; C_L: Lift coefficient; L/D: Lift to drag ratio; P_a: Power available for flight; P_r: Power required for flight; P_{ind}: Flight induced power; ΔP : Excess power available for flight (P_a–P_r); δ: Deflection of the tip of the leaf upon insect landing.; EI: Flexural stiffness; m: Body mass; g: Gravitational acceleration; F_{drag}: Drag force applying on the body in flight; F_{lift}: Lift force applying on the body in flight; DL: Wing disc loading; W_B: Body weight; A_{WD}: Wing disc area; L_w: Wing length; θ: Wing stroke amplitude; V_i: Induced velocity in the wake; LMM: Linear mixed model; CI: Confidence intervals.

Supplementary Information

The online version contains supplementary material available at https://doi.org/10.1186/s12862-022-01993-z.

Additional file 1: Table S1. Scaling relationships between body size and various morphological measurements. **Figure S1.** Morphological measurements for females (left) and males (right) *P. philippinicum*. **Figure S2.** Scaling relationships between various morphological traits (body mass (A), body area (B), body circularity (C), body aspect ratio (D), antenna length (E), front femur length (F), total wing area (G), wing loading (H) and flight muscle dry mass (I)) and body length in males (blue) and females (red). **Figure S3.** Set-up for flight trials. **Figure S4.** Analysis of a male P. philippinicum flight trial. **Figure S5.** Mean horizontal velocity (A) and mean resultant velocity (B) as a function of wing loading. **Figure S6.** Instantaneous velocity at landing as a function of male body mass. **Figure S7.** Calculation of wing stroke amplitude. **Figure S8.** Acquisition of multiple 2D photographs from different angles of a male mounted on a pin to reconstruct a single 3D model using photogrammetry. **Figure S9.** Leaf insect model and CFD simulation results.

Additional file 2: Video S1. Example of a flight trajectory from a relatively light male (374.0 mg).

Additional file 3: Video S2. Example of a flight trajectory from a relatively heavy male (504.7 mg).

Additional file 4: Video S3. Detail of a male leaf insect ascending.

Acknowledgements
The authors thank Art Woods for use of lab computer and space and Camille Thomas-Bulle and Anthony Lapsansky for useful discussions.

Authors' contributions
RPB, THB, SNG, DJE and BWT designed the study. RPB and LJK performed the flight experiments and subsequent video analyses. THB measured the attachment performance of the insects and produced the SEM images of the tarsi. RPB performed the modelling approaches and ran the statistical analyses. RPB wrote the initial manuscript, which was reviewed and edited by all authors. All authors read and approved the final manuscript.

Funding
We thank the NSF for funding (NSF award numbers, B. W. Tobalske: CMMI-1234737, D. J. Emlen: IOS 1456133 and 2015907).

Availability of data and materials
Datasets and corresponding R scripts are publicly available on Figshare: Boisseau et al. [87].

Declarations

Ethics approval and consent to participate
The experimental use of leaf insect did not require ethic approval in the United States or in Germany. Leaf insects were shipped from the Audubon Insectarium in New Orleans, Louisiana, USA and housed at the University of Montana under a USDA-APHIS permit (P526P-17-03108).

Consent for publication
Not applicable.

Competing interests
The authors declare no competing interests.

Author details
[1]Division of Biological Sciences, University of Montana, 32 Campus Dr, Missoula, MT 59812, USA. [2]Functional Morphology and Biomechanics, Zoological Institute, Kiel University, Am Botanischen Garten 9, 24098 Kiel, Germany.

Received: 12 November 2021 Accepted: 16 March 2022
Published online: 28 March 2022

References

1. Cox RM, Calsbeek R. Sexually antagonistic selection, sexual dimorphism, and the resolution of intralocus sexual conflict. Am Nat. 2009;173:176–87.
2. Fairbairn DJ, Blanckenhorn WU, Székely T. Sex, size and gender roles. Oxford: Oxford University Press; 2007. https://doi.org/10.1093/acprof:oso/9780199208784.001.0001.
3. Blanckenhorn WU. Behavioral causes and consequences of sexual size dimorphism. Ethology. 2005;111:977–1016.
4. Honěk A. Intraspecific variation in body size and fecundity in insects: a general relationship. Oikos. 1993;66:483–92.
5. Pincheira-Donoso D, Hunt J. Fecundity selection theory: concepts and evidence. Biol Rev. 2017;92:341–56.
6. Andersson M. Sexual selection. Princeton: Princeton University Press; 1994.
7. Kingsolver JG, Pfennig DW. Individual-level selection as a cause of Cope's rule of phyletic size increase. Evolution (N Y). 2004;58:1608–12.
8. Blanckenhorn WU. The evolution of body size: what keeps organisms small? Q Rev Biol. 2000;75:385–407.
9. Ghiselin M. The economy of nature and the evolution of sex. Berkeley: University of California Press; 1974.
10. Hardy ICW, Briffa M. Animal contests. Cambridge: Cambridge University Press; 2013.
11. Shuker DM, Simmons LW. The evolution of insect mating systems. Oxford: Oxford University Press; 2014.
12. Emlen ST, Oring LW. Ecology, sexual selection, and the evolution of mating systems. Science (80—). 1977;197:215–23.
13. Emlen DJ. Reproductive contests and the evolution of extreme weaponry. In: Shuker D, Simmons L, editors. The evolution of insect mating systems. Oxford: Oxford University Press; 2014. p. 92–105.
14. Herberstein ME, Painting CJ, Holwell GI. Scramble competition polygyny in terrestrial arthropods. In: Slater PJB, Beer C, editors. Advances in the study of behavior. Amsterdam: Elsevier Ltd; 2017. p. 237–95. https://doi.org/10.1016/bs.asb.2017.01.001.
15. Kelly CD. Sexual selection on size and shape in Japanese beetles (*Popillia japonica*). Behav Ecol. 2020;31:1073–83.
16. Kelly CD, Bussière LF, Gwynne DT. Sexual selection for male mobility in a giant insect with female-biased size dimorphism. Am Nat. 2008;172:417–23. https://doi.org/10.1086/589894.
17. Blanckenhorn WU, Preziosi RF, Fairbairn DJ. Time and energy constraints and the evolution of sexual size dimorphism—to eat or to mate? Evol Ecol. 1995;9:369–81.
18. Boisseau RP, Ero MM, Makai S, Bonneau LJG, Emlen DJ. Sexual dimorphism divergence between sister species is associated with a switch in habitat use and mating system in thorny devil stick insects. Behav Processes. 2020;181:104263. https://doi.org/10.1016/j.beproc.2020.104263.
19. Husak JF, Fox SF. Sexual selection on locomotor performance. Evol Ecol Res. 2008;10:213–28.
20. Biewener AA, Patek SN. Animal locomotion. Oxford: Oxford University Press; 2018.
21. Reiss MJ. The allometry of growth and reproduction. Cambridge: Cambridge University Press; 1989.
22. Barry KL. You are what you eat: food limitation affects reproductive fitness in a sexually cannibalistic praying mantid. PLoS ONE. 2013;8:e78164.
23. Hanks LM, Millar JG, Paine TD. Body size influences mating success of the eucalyptus longhorned borer (Coleoptera: Cerambycidae). J Insect Behav. 1996;9:369–82.
24. Hennemann FH, Conle OV, Gottardo M, Bresseel J. On certain species of the genus *Phyllium* Illiger, 1798, with proposals for an intra-generic systematization and the descriptions of five new species from the Philippines and Palawan (Phasmatodea: Phylliidae: Phylliinae: Phylliini). Zootaxa. 2009;2322:1–83.
25. Bradler S, Buckley TR. Biodiversity of Phasmatodea. In: Foottit RG, Adler PH, editors. Insect biodiversity: science and society. Hoboken: Wiley-Blackwell; 2018. p. 281–313.
26. Bank S, Cumming RT, Li Y, Henze K, Le Tirant S, Bradler S. A tree of leaves: phylogeny and historical biogeography of the leaf insects (Phasmatodea: Phylliidae). Commun Biol. 2021;4:1–12. https://doi.org/10.1038/s42003-021-02436-z.
27. Missbach C, Dweck HKM, Vogel H, Vilcinskas A, Stensmyr MC, Hansson BS, et al. Evolution of insect olfactory receptors. Elife. 2014;3:e02115.
28. Srinivasan G, Surendar C, Chatterjee P, Mukherjee TK. Additional records of Mantodea and Phasmida from Andaman and Nicobar Islands. Rec Zool Surv India. 2017;117:264–73.
29. Joly N. Contributions à l'histoire naturelle et à l'anatomie de la mouche-feuille des Iles Seychelles: *Phyllium crurifolium*,(Audinet Serville), *Mantis sicciofolia* (Linné). Mémoires l'Académie des Sci Toulouse. 1871;7:1–28.
30. Leigh HR. Preliminary account of the life-history of the leaf-insect, *Phyllium crurifolium* Serville. Proc Zool Soc Lond. 1909;79:103–13.
31. St Quintin WH. Notes on the life history of the leaf insects. Naturalist. 1908;618:235–8.
32. Cumming RT, Le TS, Teemsma SN, Hennemann FH, Willemse L, Büscher TH. Lost lovers linked at long last: elusive female *Nanophyllium* mystery solved after a century of being placed in a different genus (Phasmatodea, Phylliidae). Zookeys. 2020;969:43–84.
33. Zeng Y, Lin Y, Abundo A, Dudley R. Visual ecology of directed aerial descent in first-instar nymphs of the stick insect *Extatosoma tiaratum*. J Exp Biol. 2015;218:2305–14. https://doi.org/10.1242/jeb.109553.
34. Zeng Y, Chang SW, Williams JY, Nguyen LYN, Tang J, Naing G, et al. Canopy parkour: movement ecology of post-hatch dispersal in a gliding nymphal stick insect, *Extatosoma tiaratum*. J Exp Biol. 2020;223:jeb226266.
35. McCay MG. Winds under the rain forest canopy: the aerodynamic environment of gliding tree frogs. Biotropica. 2003;35:94–102.
36. Zeng Y, Malley CO, Singhal S, Rahim F, Park S, Chen X, et al. A tale of winglets: evolution of flight morphology in stick insects. Front Ecol Evol. 2020;8:121.
37. Maginnis TL. Leg regeneration stunts wing growth and hinders flight performance in a stick insect (*Sipyloidea sipylus*). Proc Biol Sci. 2006;273:1811–4.

38. Su G, Dudley R, Pan T, Zheng M, Peng L, Li Q. Maximum aerodynamic force production by the wandering glider dragonfly (*Pantala flavescens*, Libellulidae). J Exp Biol. 2020;223:218552.
39. Dudley R. The biomechanics of insect flight: form, function, evolution. Princeton: Princeton University Press; 2000.
40. Dudley R. Mechanisms and implications of animal flight maneuverability. Integr Comp Biol. 2002;42:135–40.
41. Taylor GK, Thomas ALR. Dynamic flight stability in the desert locust *Schistocerca gregaria*. J Exp Biol. 2003;206:2803–29.
42. Büscher TH, Kryuchkov M, Katanaev VL, Gorb SN. Versatility of Turing patterns potentiates rapid evolution in tarsal attachment microstructures of stick and leaf insects (Phasmatodea). J R Soc Interface. 2018;15:20180281.
43. Büscher TH, Buckley TR, Grohmann C, Gorb SN, Bradler S. The evolution of tarsal adhesive microstructures in stick and leaf insects (Phasmatodea). Front Ecol Evol. 2018;6:1–11.
44. Labonte D, Federle W. Functionally different pads on the same foot allow control of attachment: stick insects have load-sensitive "heel" pads for friction and shear-sensitive "toe" pads for adhesion. PLoS ONE. 2013;8:e81943.
45. Büscher TH, Gorb SN. Complementary effect of attachment devices in stick insects (Phasmatodea). J Exp Biol. 2019;222:jeb209833.
46. Bußhardt P, Wolf H, Gorb SN. Adhesive and frictional properties of tarsal attachment pads in two species of stick insects (Phasmatodea) with smooth and nubby euplantulae. Zoology. 2012;115:135–41. https://doi.org/10.1016/j.zool.2011.11.002.
47. Higham TE, Russell AP, Niklas KJ. Leaping lizards landing on leaves: escape-induced jumps in the rainforest canopy challenge the adhesive limits of geckos. J R Soc Interface. 2017;14:20170156.
48. Goyens J, Van Wassenbergh S, Dirckx J, Aerts P. Cost of flight and the evolution of stag beetle weaponry. J R Soc Interface. 2015;12:20150222.
49. Crandell KE, Howe RO, Falkingham PL. Repeated evolution of drag reduction at the air–water interface in diving kingfishers. J R Soc Interface. 2019;16:20190125.
50. Troelsen PV, Wilkinson DM, Seddighi M, Allanson DR, Falkingham PL. Functional morphology and hydrodynamics of plesiosaur necks: does size matter? J Vertebr Paleontol. 2019;39:e1594850.
51. Ellington CP. Limitations on animal flight performance. J Exp Biol. 1991;160:71–91.
52. Cheng B, Tobalske BW, Powers DR, Hedrick TL, Wang Y, Wethington SM, et al. Flight mechanics and control of escape manoeuvres in hummingbirds. I. Flight kinematics. J Exp Biol. 2016;219:3518–31.
53. Norberg UML, Norberg RÅ. Scaling of wingbeat frequency with body mass in bats and limits to maximum bat size. J Exp Biol. 2012;215:711–22.
54. Dudley R, Byrnes G, Yanoviak SP, Borrell B, Brown RM, McGuire JA. Gliding and the functional origins of flight: biomechanical novelty or necessity? Annu Rev Ecol Evol Syst. 2007;38:179–201.
55. Yanoviak SP, Dudley R, Kaspari M. Directed aerial descent in canopy ants. Nature. 2005;433:624–6.
56. Yanoviak SP, Munk Y, Dudley R. Evolution and ecology of directed aerial descent in arboreal ants. Integr Comp Biol. 2011;51:944–56. https://doi.org/10.1093/ICB/ICR006.
57. Büscher TH, Grohmann C, Bradler S, Gorb SN. Tarsal attachment pads in Phasmatodea (Hexapoda: Insecta). Vienna: Zoologica; 2019.
58. Varenberg M, Gorb SN. Hexagonal surface micropattern for dry and wet friction. Adv Mater. 2009;21:483–6.
59. Varenberg M, Gorb S. Shearing of fibrillar adhesive microstructure: friction and shear-related changes in pull-off force. J R Soc Interface. 2007;4:721–5.
60. Gorb S, Scherge M. Biological microtribology: anisotropy in frictional forces of orthopteran attachment pads reflects the ultrastructure of a highly deformable material. Proc R Soc B Biol Sci. 2000;267:1239–44.
61. Cumming RT, Bank S, Bresseel J, Constant J, Le Tirant S, Dong Z, et al. *Cryptophyllium*, the hidden leaf insects - descriptions of a new leaf insect genus and thirteen species from the former celebicum species group (Phasmatodea, Phylliidae). Zookeys. 2021;1018:1–179.
62. Brock PD, Büscher T, Baker E. Phasmida Species file online. Version 5.0/5.0. 2020. http://phasmida.speciesfile.org.
63. Conle OV, Hennemann FH, Perez-Gelabert DE. Studies on neotropical Phasmatodea II: Revision of the genus *Malacomorpha* Rehn, 1906, with the descriptions of seven new species (Phasmatodea: Pseudophasmatidae: Pseudophasmatinae). Zootaxa. 2008;1748:1–64.
64. Cumming RT, Bank S, Le TS, Bradler S. Notes on the leaf insects of the genus *Phyllium* of Sumatra and Java, Indonesia, including the description of two new species with purple coxae (Phasmatodea, Phylliidae). Zookeys. 2020;913:89–126.
65. Cumming RT, Leong JV, Lohman DJ. Leaf insects from Luzon, Philippines, with descriptions of four new species, the new genus *Pseudomicrophyllium*, and redescription of *Phyllium* (*Phyllium*) *geryon* Gray, 1843, (Phasmida: Phylliidae). Zootaxa. 2018;4365:101–31.
66. Cumming RT, Thurman JH, Youngdale S, Le Tirant S. *Walaphyllium* subgen nov., the dancing leaf insects from Australia and Papua New Guinea with description of a new species (Phasmatodea, Phylliidae). Zookeys. 2020;939:1–28.
67. Schneider CA, Rasband WS, Eliceiri KW. NIH Image to ImageJ: 25 years of image analysis. Nat Methods. 2012;9:671–5. https://doi.org/10.1038/nmeth.2089.
68. Hedrick TL. Software techniques for two- and three-dimensional kinematic measurements of biological and biomimetic systems. Bioinspir Biomim. 2008;3:034001.
69. R Core Team. R: a language and environment for statistical computing. 2019. https://www.r-project.org/.
70. McLean DJ, Skowron Volponi MA. trajr: an R package for characterisation of animal trajectories. Ethology. 2018;124:440–8.
71. Pohl H. A scanning electron microscopy specimen holder for viewing different angles of a single specimen. Microsc Res Tech. 2010;73:1073–6.
72. Labonte D, Clemente CJ, Dittrich A, Kuo CY, Crosby AJ, Irschick DJ, et al. Extreme positive allometry of animal adhesive pads and the size limits of adhesion-based climbing. Proc Natl Acad Sci USA. 2016;113:1297–302.
73. Bullock JMR, Drechsler P, Federle W. Comparison of smooth and hairy attachment pads in insects: friction, adhesion and mechanisms for direction-dependence. J Exp Biol. 2008;211:3333–43.
74. Wohlfart E, Wolff JO, Arzt E, Gorb SN. The whole is more than the sum of all its parts: collective effect of spider attachment organs. J Exp Biol. 2014;217:222–4.
75. Wolff JO, Gorb SN. Surface roughness effects on attachment ability of the spider *Philodromus dispar* (Araneae, Philodromidae). J Exp Biol. 2012;215:179–84.
76. Goodno BJ, Gere JM. Mechanics of materials. 9th ed. Boston: Cengage Learning; 2018.
77. Bates D, Maechler M, Bolker B, Walker S. Fitting linear mixed-effects models using lme4. J Stat Softw. 2015;67:1–48.
78. Young J, Walker SM, Bomphrey RJ, Taylor GK, Thomas ALR. Details of insect wing design and deformation enhance aerodynamic function and flight efficiency. Science (80—). 2009;325:1549–52.
79. Liang B, Sun M. Aerodynamic interactions between wing and body of a model insect in forward flight and Maneuvers. J Bionic Eng. 2013;10:19–27. https://doi.org/10.1016/S1672-6529(13)60195-X.
80. Rahman IA. Computational fluid dynamics as a tool for testing functional and ecological hypotheses in fossil taxa. Palaeontology. 2017;60:451–9.
81. Morrison FA. An introduction to fluid mechanics. New York: Cambridge University Press; 2013.
82. Epting RJ, Casey TM. Power output and wing disc loading in hovering hummingbirds. Am Nat. 1973;107:761–5.
83. Hill AV. The dimensions of animals and their muscular dynamics. Sci Prog. 1950;38:209–30.
84. Greenewalt CH. The flight of birds: the significant dimensions, their departure from the requirements for dimensional similarity, and the effect on flight aerodynamics of that departure. Trans Am Philos Soc. 1975;65:1–67.
85. Kilmer JT, Rodríguez RL. Ordinary least squares regression is indicated for studies of allometry. J Evol Biol. 2017;30:4–12. https://doi.org/10.1111/jeb.12986.
86. Schmidt-Nielsen K. Scaling: why is animal size so important? Cambridge: Cambridge University Press; 1984.
87. Romain B, Büscher TH, Douglas JE, Gorb SN, Tobalske BW. Phyllium locomotion 2022_data and scripts.zip. figshare. 2021. https://doi.org/10.6084/m9.figshare.14852904.v3

Publisher's Note